Signal and noise characteristics of SSFP FMRI: A comparison with GRE at multiple field strengths

Karla L. Miller,[a,*] Stephen M. Smith,[a] Peter Jezzard,[a] Graham C. Wiggins,[b] and Christopher J. Wiggins[b]

[a]*Centre for Functional MRI of the Brain (FMRIB), University of Oxford, Oxford, UK*
[b]*A.A. Martinos Center, Massachusetts General Hospital, Charlestown, MA, USA*

Recent work has proposed the use of steady-state free precession (SSFP) as an alternative to the conventional methods for obtaining functional MRI (FMRI) data. The contrast mechanism in SSFP is likely to be related to conventional FMRI signals, but the details of the signal changes may differ in important ways. Functional contrast in SSFP has been proposed to result from several different mechanisms, which are likely to contribute in varying degrees depending on the specific parameters used in the experiment. In particular, the signal dynamics are likely to differ depending on whether the sequence is configured to scan in the SSFP transition band or passband. This work describes experiments that explore the source of SSFP FMRI signal changes by comparing SSFP data to conventional gradient-recalled echo (GRE) data. Data were acquired at a range of magnetic field strengths and repetition times, for both transition band and passband methods. The signal properties of SSFP and GRE differ significantly, confirming a different source of functional contrast in SSFP. In addition, the temporal noise properties are significantly different, with important implications for SSFP FMRI sequence optimisation.

Introduction

Most functional MRI (FMRI) data are acquired using gradient-recalled echo (GRE) pulse sequences with single-shot echo planar imaging (EPI) acquisitions. This method uses a long echo time (T_E) to sensitise the sequence to blood oxygenation level dependent (BOLD) signal changes and single-shot EPI to obtain reasonable temporal resolution. While highly efficient, GRE-EPI suffers from signal dropout due to long T_E and heavy image distortion due to the long, single-shot readout. These artefacts limit the achievable resolution and effectively preclude imaging in certain regions of the brain (e.g., prefrontal lobe).

* Corresponding author. FMRIB Centre, John Radcliffe Hospital, Headington, Oxford, OX3 9DU, UK. Fax: +44 1865 222717.
E-mail address: karla@fmrib.ox.ac.uk (K.L. Miller).
Available online on ScienceDirect (www.sciencedirect.com).

Balanced steady-state free precession (SSFP) is a pulse sequence that combines short readout durations with fast and efficient imaging, properties that are desirable in FMRI. Several recent studies have demonstrated the ability to obtain functional contrast with SSFP (Scheffler et al., 2001; Miller et al., 2003; Bowen et al., 2005). These methods are able to obtain BOLD-like functional contrast at short T_E and use rapid multi-shot readouts with a short repetition time (T_R). These methods should therefore be relatively immune to the image distortion and signal dropout found in single-shot GRE-EPI.

Although previous work has demonstrated the ability to acquire FMRI contrast with SSFP, the signal characteristics, including the source of contrast, have not been carefully studied. Several sources of contrast have been proposed depending on the details of the SSFP acquisition, including direct detection of the BOLD frequency modulations (Scheffler et al., 2001; Miller et al., 2003), diffusion in the extravascular space (Bowen et al., 2006) and T_2^* effects at long T_R (Zhong et al., 2007). Because the SSFP signal has a fairly complicated dependence on all these effects, they are all likely to contribute to varying degrees depending on the details of the SSFP acquisition; however, no detailed characterisation has previously been performed to study these affects.

In addition to potential sources of functional contrast in SSFP, noise characteristics are also important for pragmatic reasons. It has previously been established that sources of temporal frequency drift (e.g., from respiration (Lee et al., 2006) or gradient heating (Miller et al., 2006; Wu et al., 2007)) can introduce significant temporal instability. Although methods for reducing these drifts using real-time feedback have been suggested (Lee et al., 2006; Wu et al., 2007), no detailed characterisation of the noise has previously been reported.

In this work, we attempt to clarify some of these issues by characterising the functional contrast and temporal noise in SSFP FMRI. This characterisation is primarily based on matched SSFP and GRE experiments, which use the well-studied GRE signal as a reference for T_2^* BOLD signal. We also compare the noise sensitivity of the different methods by fitting a model for physiological noise in FMRI (Krüger and Glover, 2001) to the experimental data.

Theory

FMRI with Balanced SSFP

Balanced SSFP has two defining characteristics. First, use of a short T_R ($T_R < T_2$) causes the transverse magnetisation to persist over multiple repetition periods. Second, all gradient waveforms have zero total area over the T_R, such that any phase accumulated during the T_R is purely due to off-resonance precession. The combined effect of these properties is that the resultant steady-state signal has a strong dependence on the relationship between the signal phase (due to off-resonance precession) and the RF excitation phase (which is typically incremented from one excitation to the next).

The dependence of the balanced SSFP signal on the local resonance frequency is demonstrated in Fig. 1 for two flip angles. The reference frequency (0 Hz in Fig. 1) corresponds to the absolute frequency for which the off-resonance phase accrual during the T_R is exactly matched by the RF phase increment. Thus, the signal profile can be shifted relative to some absolute frequency by changing the RF phase increment. The plots in Fig. 1 are calculated with no applied phase increment; in structural imaging, is common to acquire with a high flip angle and set the reference frequency such that mean object frequency lies in the centre of the broad passband in Fig. 1b.

Current balanced SSFP methods for FMRI can be divided into two categories, based on the setting of the reference frequency relative to local tissue frequency. The earlier methods aim to use the frequency sensitivity of the SSFP signal to detect the deoxyhemoglobin frequency shift directly (Scheffler et al., 2001; Miller et al., 2003). These methods set the reference frequency such that tissue lies in the part of the SSFP signal profile with maximal sensitivity to off-resonance (i.e., in the region where the signal profile has greatest gradient). Because this functional signal is maximised in the frequency band with the sharpest signal transition, these methods focus on the transition ban and will be referred to as "transition band SSFP", or tbSSFP. More recently, it has been demonstrated that FMRI contrast can be achieved in the flat passband portion of the SSFP signal profile, which will be referred to as "passband SSFP", or pbSSFP (Bowen et al., 2005). Different sources of contrast for pbSSFP have been proposed (Bowen et al., 2006; Zhong et al., 2007), and it is likely to be more similar to conventional BOLD FMRI than to tbSSFP. The transition band and passband are indicated for low and high flip angle in Fig. 1.

Previous work has demonstrated the feasibility of detecting activation with balanced SSFP, but to date only limited work has been done to investigate the source of SSFP FMRI signals. One study measured passband SSFP FMRI at a range of T_E and T_R, finding that signal changes at long T_R are dominated by T_2^* BOLD effects (Zhong et al., 2007). Another study of passband SSFP FMRI seems to indicate that diffusion effects, not T_2^*, dominate at short T_R (Bowen et al., 2006). In addition, there has been some theoretical treatment of passband SSFP oxygenation contrast in other organs (Dharmakumar et al., 2006), which describe apparent T_2 contrast in baseline (i.e., resting) signal levels resulting from exchange across red blood cell membranes. Qualitative descriptions of the proposed source of signal changes in transition-band SSFP have been described due to both magnitude (Scheffler et al., 2001) and dephasing effects (Miller et al., 2003), but no detailed studies of these effects have been conducted.

Matching GRE and SSFP Acquisitions

This study utilises a pulse sequence that converts balanced SSFP to GRE with the addition of a spoiler gradient, shown in
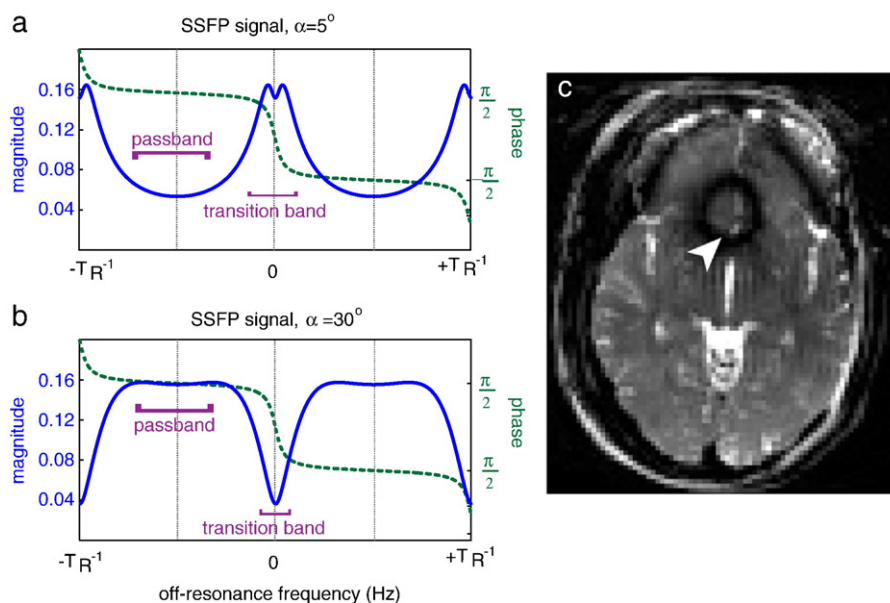
Fig. 1. (a, b) Balanced SSFP signal plotted over a range of off-resonance frequencies. Balanced SSFP signal magnitude (blue solid lines) and phase (green dashed lines) have a strong dependence on local resonance frequency. In this work, the band of frequencies exhibiting relatively constant signal is referred to as the passband, and the band of frequencies with rapidly changing signal is referred to as the transition band. At low flip angle, the signal peaks in the transition band (a), whereas at high flip angle, the highest signal occurs in the passband (b). (c) Balanced SSFP images (here, with $\alpha = 30°$) exhibit unusual contrast based on the signal pattern shown in panel b. If the frequency is set such that the majority of the brain lies in the passband, some regions of the brain will lie in the transition band due to an imperfect shim, leading to characteristic low-signal bands in the image (arrow).

Fig. 2. A slab-selective excitation is followed by a 3D stack-of-segmented EPI readout (Miller et al., 2006), in which segmented EPI is acquired with additional phase encoding along the third dimension (k_z in Fig. 2). The imaging gradients are refocused, and then followed by an optional spoiling gradient that converts the sequence between balanced SSFP (spoiling off) and GRE (spoiling on). The location of the passband and transition band is controlled by changing the phase increment of the excitation pulse.

This sequence enables each SSFP data set to be accompanied by a matched GRE acquisition with identical scan parameters. The GRE data can be thought of as matched to SSFP in all senses, except that the echo pathways from previous excitations are attenuated (i.e., converted to high-order configurations; Hennig, 1991), removing the SSFP banding. Most significantly, the T_2^* effects that result in conventional BOLD contrast are matched in SSFP and GRE, allowing the GRE data to serve as an estimate of the T_2^* effects present in the SSFP data. A similar method has previously been used in passband SSFP to characterise vascular signal contributions (Bowen et al., 2005).

Temporal noise model

The source of functional contrast is one important aspect of the SSFP FMRI signal. Equally important are the temporal noise properties and their effect on the resulting contrast-to-noise ratio (CNR), which determines the statistical robustness of the signal. Previous work has demonstrated that transition band SSFP has strong sensitivity to temporal frequency drift due to physiological effects (Lee et al., 2006). However, fairly little work has been done to characterise this noise in SSFP FMRI.

Noise in conventional FMRI is typically described using the Krüger noise model (Krüger and Glover, 2001). This model accounts for both thermal noise (which is independent of image signal level) and physiological noise (which scales with image signal level). Given a measure of the image SNR (SNR_0), the time series SNR (tSNR) can be modeled using:

$$\text{tSNR} = \frac{\text{SNR}_0}{\sqrt{1 + \lambda^2 \text{SNR}_0^2}} \qquad (1)$$

where λ accounts for the component of the noise that scales with image SNR. The value of λ determines the maximum achievable

tSNR (i.e., the asymptotic limit on tSNR as SNR_0 increases; Krüger and Glover, 2001), with a small λ indicating less physiological noise and a greater maximum tSNR. One goal of this work is to consider whether this model is appropriate for SSFP and, if so, to compare the noise properties of SSFP and GRE based on the term λ.

Methods

Two experiments were performed to separately compare transition band and passband SSFP with matched GRE reference data. The matched GRE data provide a useful measure of the T_2^* BOLD effects present in the SSFP data. These studies aimed to elucidate the source of functional contrast in SSFP, as well as the relative sensitivity to noise sources.

In most balanced SSFP methods, the relationship $T_E = T_R/2$ is imposed, largely to achieve a maximally efficient acquisition, but also in part because the balanced SSFP signal usually exhibits a "spin echo" at this T_E (Scheffler and Hennig, 2003). All experiments in this paper are acquired with this approximate relationship. Nevertheless, because this relationship is not generally true in conventional FMRI, we will refer to both T_E and T_R whenever possible. When T_E or T_R of SSFP are referred to in isolation, it is for convenience and the assumption of $T_E = T_R/2$ holds.

It is important to note that these experiments are not intended to serve as a comparison of SSFP FMRI with conventional GRE BOLD acquisitions but rather to use the matched GRE data as a tool for separating T_2^* effects from other sources of functional contrast in SSFP. The acquired GRE data differ from conventional BOLD in that it is acquired with relatively short T_E using a 3D k-space trajectory at a flip angle optimised for SSFP. It is therefore not advised to draw conclusions on the relative CNR of SSFP and GRE BOLD from the present study.

Stimulation paradigm

All studies utilised the same visual stimulation paradigm. A blue/yellow annular checkerboard pattern reversing at 8 Hz was interspersed with rest periods consisting of a black background with a white cross fixation point. This stimulus was presented in a block paradigm with 15 s of rest followed by 15 s of stimulation, repeated 4 times (2 min total).

Transition band SSFP vs. GRE Protocol

Fifteen healthy human subjects were studied on Siemens 1.5 T, 3 T and 7 T scanners (5 different subjects at each field). Subjects were scanned during visual stimulation using GRE and tbSSFP protocols each at $T_E/T_R = 6/12$ and 18/36 ms. Images were acquired with resolution $2 \times 2 \times 2$ mm³, with slightly different imaging parameters at 7 T due to the different gradient hardware (see Table 1). The flip angle was chosen to maximise transition band SSFP functional contrast ($\alpha = 4°/7°$ for $T_R = 12/36$ ms, about half the Ernst angle for the GRE runs). For each protocol, three 2-min runs were acquired, for a total of 12 runs per subject. The shim volume was localised to the occipital pole, and the phase increment was changed in each run such that the reference frequency for each run was shifted by 4–6 Hz (covering a total of 12–24 Hz over three runs), optimised to provide full coverage of the visual cortex (Miller et al., 2003). The same three frequencies were used in both

Fig. 2. Pulse sequence utilised in this study. Following slab-selective excitation (a), a 3D stack-of-segmented EPI acquisition is used (b, the readout is along k_x, EPI phase encoding blips are along k_y and 3D phase encoding is along k_z). All imaging gradients are rewound after the readout (c). Finally, an optional spoiler gradient after the readout (d) converts the sequence from balanced SSFP (spoiling off) into GRE (spoiling on).

Table 1
Image acquisition parameters for the tbSSFP vs. GRE comparison experiment

		$T_R = 12$ ms	$T_R = 36$ ms
1.5 T, 3 T	FOV	$192 \times 192 \times 40$ mm^3	
	Matrix	$96 \times 96 \times 20$	
	BW	1002 Hz/pix	1302 Hz/pix
	T_{vol}	2.9 s	4.8 s
7 T	FOV	$192 \times 192 \times 32$ mm^3	
	Matrix	$96 \times 96 \times 16$	
	BW	1240 Hz/pix	1408 Hz/pix
	T_{vol}	2.4 s	4.2 s

Slightly different parameters at 7 T were used due to the different gradient capabilities of that system.

tbSSFP and GRE to exactly match the acquisitions, although GRE contrast should not depend on phase increment.

Passband SSFP vs. GRE protocol

Ten healthy human subjects were studied at 1.5 T and 3 T (5 different subjects at each field) using GRE and pbSSFP protocols at $T_R = 7.3, 13, 25, 36, 50$ ms and $T_E = T_R/2$. Compared to the transition band experiment, we were able to accommodate a larger number of T_R, primarily because there is no need to acquire multifrequency data provided a good shim is achieved in the visual cortex (an advantage of the passband method). However, it was decided to acquire larger voxels ($2.9 \times 2.9 \times 3.0$ mm^3) to improve the SNR of each short run. Flip angle was set to create a maximally flat passband region in SSFP ($\alpha = 30°$). The shim volume was localised to the occipital pole, and the reference frequency was set to avoid any banding in this region. Other parameters are given in Table 2.

Data analysis

All data were analysed using the FSL software package (Smith et al., 2004). Within-run motion correction was not used in order to avoid introducing misalignment due to fluctuating SSFP banding patterns. Instead, subjects were comfortably restrained with soft padding at the temples. All data were visually inspected to ensure that motion was minimal, and any subject exhibiting significant motion was discarded (this was only necessary for two out of 25 subjects, who were re-scanned at a later date). Data were high-pass filtered with full-width at half-maximum of 30 s (it is safe within FEAT to set the FWHM to the paradigm frequency because the filter has a smooth roll-off in the frequency domain). These filtered data were analysed with the standard general linear model using the canonical hemodynamic response function and including temporal derivative terms to account for slight temporal shifts.

Each subject's data was aligned across separate runs using rigid-body alignment (6 degrees-of-freedom). In general, acquisition parameters were optimised for efficiency, so that longer T_R was associated with longer EPI readouts (e.g., more lines per segment). This should enable direct SNR and CNR comparison for runs of the same total duration, but leads to different distortions in the long and short T_R data. Thus, alignments utilised a mask over the occipital lobe to enforce good alignment in the visual cortex at the expense of poor alignment in distal regions. All alignments were carefully verified by eye.

Following standard GLM analysis, a region-of-interest (ROI) was defined by thresholding the fixed-effects (FE) z-statistic across all runs of all methods ($z_{FE} \geq 2.0$, where z_{FE} is proportional to the mean z-statistic across the different runs). Thermal SNR (SNR$_0$), time course SNR (tSNR), functional CNR, relative signal change (ΔS) and time series noise (η) were calculated as follows. The functional CNR is proportional to the z-statistic of the GLM fitting (due to the simple block design and large number of time points). Relative signal change (ΔS) is given by the fitted parameter estimate divided by the mean time course signal. Time series noise (η) is calculated as the standard deviation of the GLM residuals divided by the mean signal level. Finally, thermal SNR (SNR$_0$) and time course SNR (tSNR) were calculated using the activation ROI and a 1000-voxel background region as:

$$\text{SNR}_0 = \frac{\mu_{ROI}}{\sigma_{bg}} \quad (2)$$

$$\text{tSNR} = \frac{\mu_{ROI}}{\sigma_\eta} = \frac{1}{\eta} \quad (3)$$

where μ_{ROI} is the mean signal within the activation ROI, σ_{bg} is the standard deviation in the background region and σ_η is the standard deviation of the GLM residuals within the ROI. Note that tSNR and time series noise (η) are reciprocal values, but both are specified because each is useful in a different context.

Noise model fitting

The Krüger model for time series SNR given in Eq. (1) was separately fit to the SSFP and GRE data within the ROI using the SNR$_0$ and tSNR quantities as defined above. These fits used only the 1.5 T and 3-T data because the SNR$_0$ varies significantly across the 7-T images due to B1 inhomogeneity. In order to accurately fit the noise model, it is crucial to account for the discrepancy in thermal noise variance in a region with low signal compared to a high-signal region (i.e., the Rician noise distribution) (Gudbjartsson and Patz, 1995). One common approach is to assume that the complex signal in the background has zero mean, in which case one should correct by a factor of $\sqrt{2 - \pi/2}$ (Triantafyllou et al., 2005). In our data, the background noise was poorly described by a zero-mean Rician distribution (potentially due to diffuse aliased signal), introducing a negative bias to our SNR$_0$ calculations that was sufficient in a few cases to cause the physically impossible measurement SNR$_0 <$ tSNR. An improved estimate of σ_{bg} was

Table 2
Image acquisition parameters for the passband SSFP vs. GRE comparison experiment

	T_E/T_R (ms)				
	3/7	6/13	12/25	18/36	25/50
FOV(mm^2)	260×176		260×255		
Matrix	$90 \times 60 \times 24$		$90 \times 88 \times 24$		
PE dir.	R/L		A/P		
BW(Hz/pix)	1852	1502		1462	
n_{seg} (s)	20	9	5	3	3
T_{vol} (s)	3.7	2.8	3.0	2.6	3.6

Slightly different parameters at short T_R were necessary to achieve the same coverage and resolution in similar times.

obtained by fitting the background noise histogram to a Rician distribution with non-zero mean. Non-linear fits were performed in Matlab (using the nlinfit function) and were found to have an acceptable confidence interval (typically 5–10%, although occasionally as high as 30%).

Results

Transition band SSFP vs. GRE

Example activation maps are shown in Fig. 3, where the top row shows the multi-frequency data from a single subject at 3 T and $T_R = 12$ ms, and the bottom row shows thresholded fixed-effects activation maps for each condition in a different subject at 3 T. These images demonstrate increased SSFP banding at longer T_R, reduced GRE contrast at short T_R and higher distortion in both SSFP and GRE at long T_R. The ROIs are created by a fixed-effects combination of the activation maps from the different conditions (i.e., an FE analysis of the activation maps in the lower row of Fig. 3, which is equivalent to a single-level FE analysis of all data). Across the different subjects, the ROIs contained 18–134 (39 ± 37) voxels at 1.5 T, 294–767 (560 ± 183) voxels at 3 T and 436–2233 (1183 ± 659) voxels at 7 T.

Fig. 4 presents a group analysis pooling subjects within conditions including significance testing (subject-wise paired *t*-tests comparing tbSSFP vs. GRE). Individual results are presented as Supplementary Fig. 9, including significance testing (voxel-wise paired *t*-tests of tbSSFP vs. GRE within each subject) to demonstrate the good inter-subject reproducibility.

SNR_0 was significantly higher in tbSSFP than in GRE at 1.5 T and 3 T, as expected in the high-signal SSFP bands where the functionally determined ROI occurs. This SNR_0 difference was insignificant at 7 T. At this field strength, the tbSSFP images qualitatively appeared to exhibit less-distinct bands, which seemed to indicate that the signal was not forming a robust SSFP condition due to the broader line spread. SNR_0 of both sequences varies approximately linearly with field strength, as would be expected, except for anomalously high SNR_0 in the tbSSFP short T_R data at 3 T.

The relative signal change (ΔS) in tbSSFP was found to be significantly higher than GRE at 1.5 T and 3 T, but the tbSSFP and GRE signal changes converged at 7 T. A related trend can be seen in comparing short vs. long T_R data, where the SSFP and GRE signal changes were closer at long T_R than at short T_R. These trends are likely to reflect an increase in T_2^* BOLD contrast in balanced SSFP as either T_E or field strength increase. At one extreme is the data at 1.5 T with short T_R, where the tbSSFP signal change is approximately four times the GRE signal change, indicating that a contrast mechanism other than T_2^* dominates. At the other extreme is the data at 7 T, where the two sequences have essentially the same relative signal change, suggesting a T_2^* effect for both. It is also interesting to note that tbSSFP signal change reduces with increasing field strength, whereas the GRE signal change increases until they converge. This indicates that as the T_2^* effects are increasing, the non-T_2^* source of contrast in tbSSFP is reduced.

Time series noise (η) is also significantly higher in tbSSFP than GRE, with tbSSFP noise increasingly dominant at high field strength. This same trend can be seen in Fig. 5, which shows the fit of the Krüger SNR model to the tbSSFP and GRE data (excluding the 7-T results, as discussed above). The fitted value of λ for GRE

($\lambda = 1.1\%$) is in good agreement with literature values (typically $\lambda = 1.2\%$; Krüger and Glover, 2001; Triantafyllou et al., 2005). The fitted value for tbSSFP ($\lambda = 2.4\%$) reflects the larger signal fluctuations due to physiological noise (which can also be seen in the raw data, for example Supplementary Fig. 9). However, it is immediately apparent that the fitted Krüger model has greater residual error for the tbSSFP data. This was true even when discarding outlier data sets and fitting to reduced subsets of the data (e.g., using only short or long T_R data). These poor fits may be indicative of different temporal noise processes in tbSSFP, as discussed below.

The CNR reflects a combination of ΔS and η, favoring tbSSFP at low field due to greater signal contrast and GRE at high field due to lower noise. These results indicate that the bands in transition band SSFP both contribute functional contrast (beyond the T_2^* effects present in the GRE data) and reduce temporal stability.

The effect of field strength was assessed using paired *t*-tests (subject-wise paired *t*-tests comparing field strengths), as shown in Table 3. Most of the statistical measures exhibited significant field strength dependence ($p < 0.05$). The notable exceptions are that tbSSFP CNR is not significantly different at 1.5 T and 3 T, and that the tbSSFP percent signal change tends not to be significantly affected by a change in field strength.

Passband SSFP vs. GRE

Example images acquired with passband SSFP at the longest and shortest T_R are shown in Fig. 6. The fixed-effects analysis of all data resulted in ROIs with 1628–3603 (2559 ± 943) voxels at 1.5 T and 3710–5404 (4504 ± 890) voxels at 3 T. Fig. 7 shows results of the ROI analysis on the passband SSFP data. Individual subject results at 3 T, shown in Supplementary Fig. 10, demonstrate excellent reproducibility across subjects (similar results were found at 1.5 T, not shown). Fig. 7 reduces the data from each subject in each condition to a single mean across the ROI, which were then tested for significance. The functional contrast (ΔS) for pbSSFP and GRE is different for short T_E/T_R and converges at long T_E/T_R. Although the divergence of the GRE and pbSSFP signal curves at short T_E/T_R is subtle, it is also highly significant across the group ($p < 0.001$ at both field strengths).

The fact that the signal converges with T_2^*-based GRE data at long T_R supports previous work on SSFP FMRI which modeled signal at long T_R and a range of T_E, concluding that changes at long T_R were primarily due to T_2^* (Zhong et al., 2007). The divergence of SSFP and GRE data at short T_R indicates a different contrast mechanism for SSFP in this regime. While GRE data would not be expected to exhibit signal changes at very short T_E, balanced SSFP has T_2 contrast due to refocused spin and stimulated echoes from previous T_R (Hennig, 1991).

The CNR of passband SSFP (Figs. 7a and c) is relatively independent of T_E, while the CNR of GRE decreases rapidly as the echo time approaches zero. Similar dynamics are observed at 1.5 T and 3 T. The ability to achieve high SNR at short T_R is a recognised benefit of passband SSFP (Reeder et al., 2004), and it is interesting to note that this property extends to CNR in pbSSFP FMRI.

Fig. 8 shows the fit of the Krüger SNR model to the pbSSFP and GRE data. Fig. 8a shows the model fit to the GRE and pbSSFP pooled data from all T_R. The model provides a good fit to the GRE data (in red), with $\lambda = 1.0\%$ in good agreement with literature
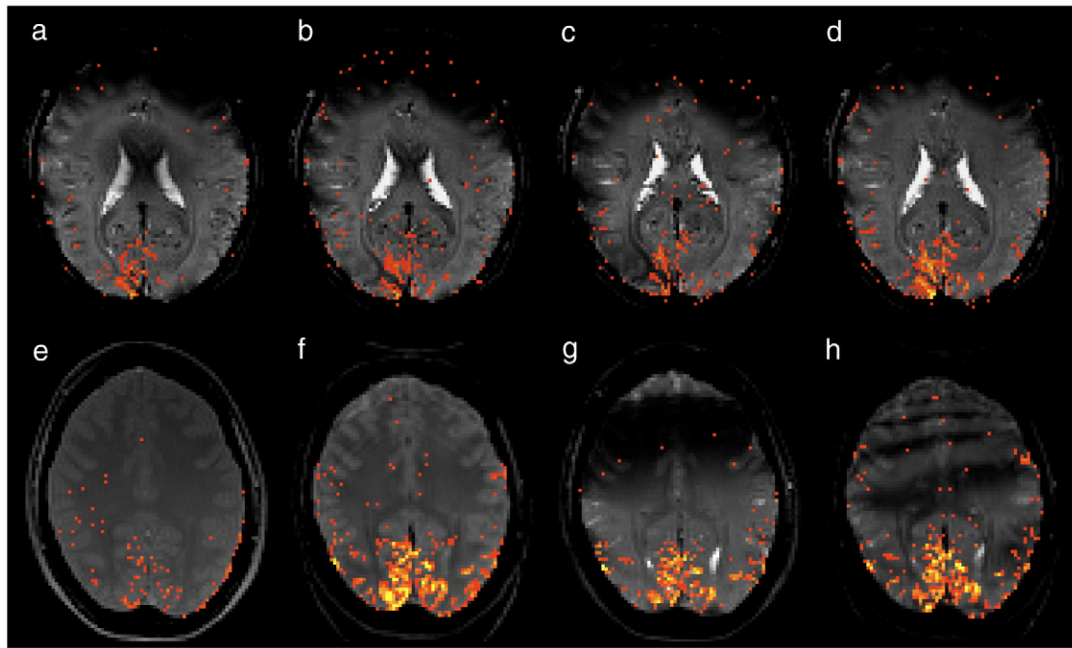
Fig. 3. Example data from the transition band SSFP experiment at 3 T, illustrating individual SSFP runs at different frequencies (top row) and the fixed-effects analysis over multiple frequencies for each of the four conditions (bottom row). Activation maps are overlaid on the mean time course image (for a single frequency) or the mean-of-time-course-means (for combined data). The top row shows example multi-frequency data from a typical subject at $T_E/T_R=6/12$ ms for (a) 0 Hz, (b) 4 Hz and (c) 8 Hz frequency offset, and (d) the fixed-effects combination over all three frequencies. The shift in SSFP bands is visible in panels a–c. The bottom row shows the combined (FE) analysis for a different subject for (e) GRE at $T_E/T_R=6/12$ ms, (b) GRE at $T_E/T_R=18/36$ ms, (c) SSFP at $T_E/T_R=6/12$ ms, (d) SSFP at $T_E/T_R=18/36$ ms. Increased SSFP banding and higher distortion are visible in the long T_R data.

values ($\lambda=1.2\%$; Krüger and Glover, 2001; Triantafyllou et al., 2005). However, the model clearly does a poor job of describing the pbSSFP data (blue). On further inspection, it was noted that the

tSNR in SSFP had a strong dependence on the T_R at which it was acquired, and that this dependence was not simply due to variation in SNR_0. Fig. 8b shows the Krüger model fit using only the data at
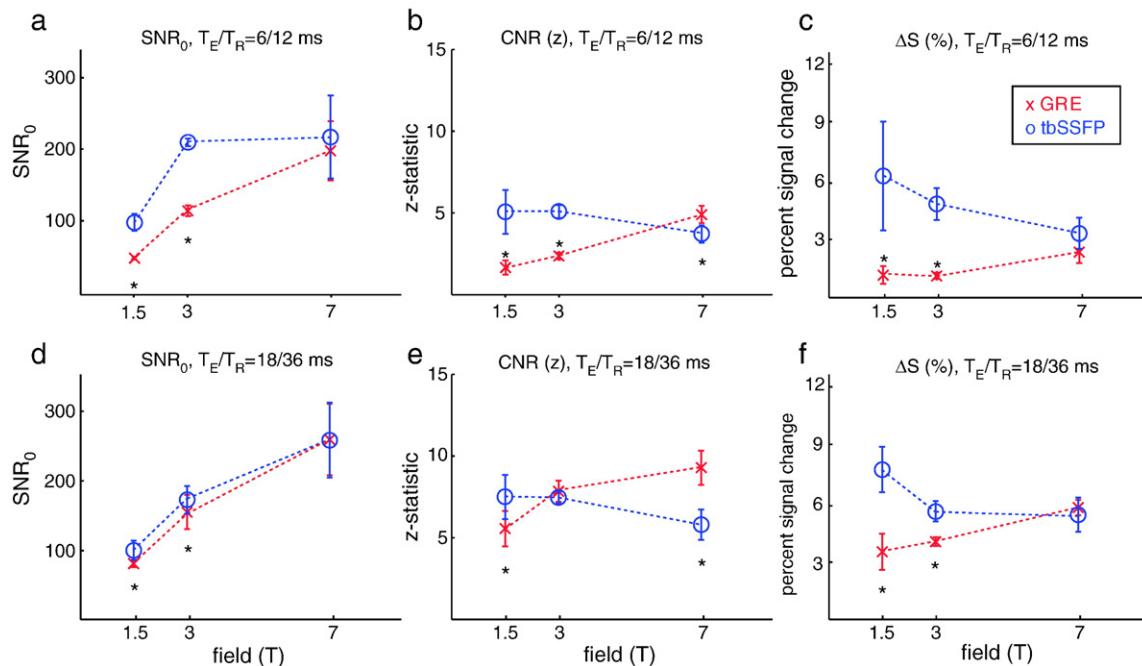
Fig. 4. Group results for the transition band SSFP (blue) vs. GRE (red) comparison study. Data for the five subjects at each field strength are pooled and represented as group mean±SD. The top row are data for $T_E/T_R=6/12$ ms and the bottom row are data for $T_E/T_R=18/36$ ms. Plotted values are (a, d) SNR_0, (b, e) CNR and (c, f) ΔS. This figure demonstrates the variation in the different statistical measures over the range of field strengths. Asterisks indicate significance in a subject-wise paired t-test between tbSSFP and GRE.
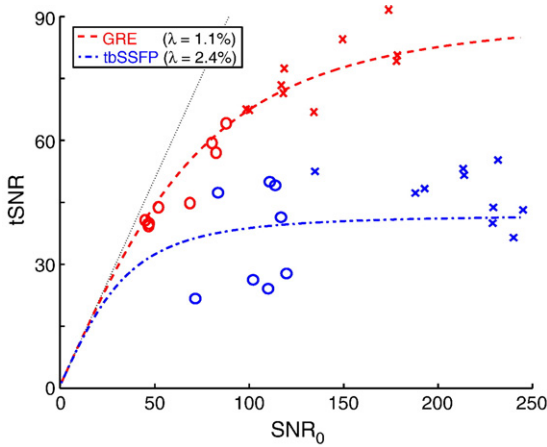
Fig. 5. Results of fitted Krüger SNR model to transition band SSFP (blue) and GRE (red) data. Individual points depict a single subject mean over the functional ROI. The line of identity ($SNR_0 = tSNR$) is shown in gray, data at 1.5 T are indicated by a circle and data at 3 T are indicated by a cross. The fitted λ value for GRE is in good agreement with literature; the λ fitted to transition band SSFP indicates roughly twice the physiological noise. However, the Krüger SNR model fit to the SSFP data has a fairly high fitting error, which may indicate different temporal noise processes.

short T_R ($T_R = 6-12$ ms). This subset of the SSFP data is well described by the Krüger model, although the fitted $\lambda = 0.4\%$ is much smaller than that usually fitted to GRE. The fitted $\lambda = 1.1\%$ for short T_R GRE data is essentially the same as is fitted to the entire data set. Fig. 8c shows a similar plot for the model fit using only the data at long T_R ($T_R = 36-50$ ms). Here, the GRE and SSFP data are fit to a similar λ, although the fit to the SSFP data has higher residual error.

Fig. 8d plots the value for λ fitted to data at different T_R for GRE and SSFP (with the error bars indicating the 95% confidence interval for the fit). Each fit pools the data from two consecutive T_R in order to achieve a robust fit, as data from a single T_R were insufficient. The value of λ fitted to the GRE data is largely independent of the T_R, as would be predicted by the Krüger model. However, the value of λ fitted to the pbSSFP data has a strong dependence on T_R. This would seem to indicate that pbSSFP has a low sensitivity to physiological noise at short T_R but similar (or potentially higher) sensitivity to GRE at long T_R. This may reflect different noise sensitivity in T_2 BOLD contrast compared to T_2^* BOLD contrast.

Discussion

In this paper, we have described the first comprehensive characterisation of SSFP FMRI signal over a broad range of imaging conditions. The signal dynamics that lead to functional contrast in SSFP are shown to be more complicated than in GRE acquisitions, where signal changes are typically assumed to result solely from T_2^* BOLD effects. The SSFP signal is partly composed of stimulated echoes with fairly long mixing times, which achieve effective echo times that are longer than T_E and thus contain significant T_2 weighting. SSFP at short T_R may therefore exhibit T_2 BOLD contrast. The chemical shift of deoxyhemoglobin may also interact with the sensitivity of the SSFP signal to resonance frequency by creating signal changes that directly reflect the deoxyhemoglobin chemical shift (i.e., these signal changes occur at

the level of spin isochromats, rather than T_2^* signal dephasing across multiple isochromats).

The SSFP–GRE comparison experiments aim to qualitatively separate the relative contributions of T_2^*, T_2 and chemical shift effects in SSFP FMRI. Functional contrast in the reference GRE data is assumed to result solely from T_2^* BOLD effects. The difference between GRE and SSFP functional contrast at a given T_E is therefore expected to reflect T_2 and/or chemical shift BOLD effects, while the GRE functional contrast provides a measure for the contribution from T_2^* BOLD in both sequences. Although passband and transition band SSFP are both likely to contain some T_2 and some chemical shift contribution, it is useful to assume that passband SSFP contains minimal chemical shift sensitivity (due to the flat signal profile in the passband) and conversely that transition band SSFP contains minimal T_2 contrast (or, more accurately, that T_2 dynamics are lumped in with chemical shift effects in the transition band due to the complicated signal dynamics in this part of the spectrum). The discussion below will use this assumption but should be viewed in light of the fact that both chemical shift and T_2 effects contribute in varying degrees to any SSFP FMRI acquisition.

Transition band SSFP

Each pair of matched tbSSFP-GRE experiments indicates whether the presence of the SSFP signal bands improves functional contrast or introduces noise; in general both occur, and the CNR reflects the resulting balance. At low and medium field, tbSSFP has higher contrast than GRE (ΔS in Fig. 4), indicating that tbSSFP contrast results in part due to the presence of SSFP bands. At high field and long T_E/T_R, the relative signal changes in tbSSFP and GRE converge, which likely indicates a convergence in contrast mechanism to a T_2^* BOLD effect.

One interesting effect in the tbSSFP data is the reduction in ΔS with increasing field strength, whereas conventional BOLD contrast in GRE increases with field strength (both effects can be seen in Figs. 4c, f). As discussed above, this would seem to indicate that as T_2^* BOLD contrast increases in tbSSFP (either due to longer T_E or higher field strength), the additional source of contrast in tbSSFP is reduced, causing the GRE and tbSSFP curves to converge. One interesting consequence of this dependence is that it is not consistent with additional contrast from T_2 changes, which are the most likely source of contrast at short T_R in passband SSFP. Assuming that the non-T_2^* contrast in tbSSFP is introduced by the presence of SSFP bands, the above effect could be caused by a reduction in banding at long T_E/T_R and high field. At high field and long T_R, the intra-voxel line spread is broad relative to the

Table 3
Significance for paired *t*-tests of field strength effects in tbSSFP

		SNR_0		CNR (z)		ΔS (%)	
		GRE	tbSSFP	GRE	tbSSFP	GRE	tbSSFP
$T_R = 12$ ms	1.5 T vs. 3 T	***	***	*	0.97	0.90	0.43
	3 T vs. 7 T	*	0.82	***	*	*	0.09
	1.5 T vs. 7 T	***	*	***	0.12	***	0.21
$T_R = 36$ m	1.5 T vs. 3 T	**	**	*	0.95	0.36	**
	3 T vs. 7 T	*	*	*	*	***	0.80
	1.5 T vs. 7 T	**	*	*	0.17	*	*

Significance is indicated by asterisks ($*p < 0.05$, $**p < 0.01$, $***p < 0.005$); otherwise the *p*-value is given.
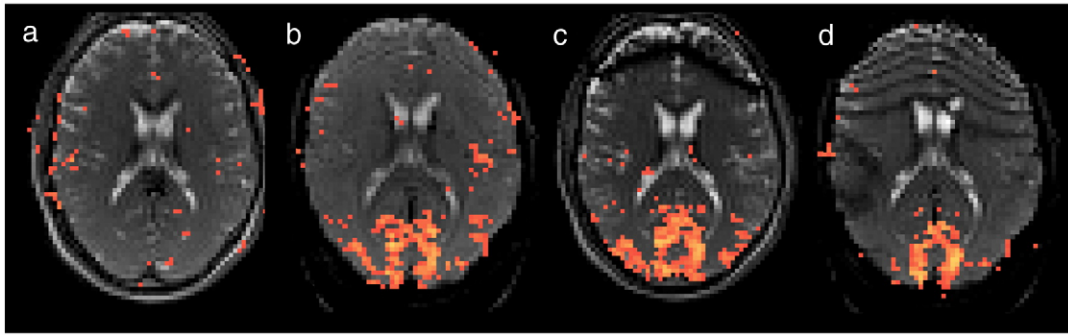
Fig. 6. Example activation maps at 3 T for the passband SSFP experiments. The activation maps from the pbSSFP experiment are for (a) GRE at $T_E/T_R = 3/7$ ms, (b) GRE at $T_E/T_R = 25/50$ ms, (c) pbSSFP at $T_E/T_R = 3/7$ ms and (d) pbSSFP at $T_E/T_R = 25/50$ ms. The SSFP images exhibit banding in the frontal lobes, which increases at long T_R, due to the targeting of the shim to the occipital lobe. Many subjects also exhibit increased distortion at long T_R in the frontal lobes, although this particular subject did not.

width of the SSFP bands and will effectively blur the banding pattern (Scheffler et al., 2001). These blurring effects were observed in our data (particularly at 7 T, where banding was clearly reduced).

The reduced banding in the SSFP images at 7 T may indicate that the signal is only partially in the balanced SSFP condition at this field strength. In this case, the presence of SSFP bands seem to primarily introduce instability to the signal. Although these results suggest that SSFP may not be well-suited to 7 T, they do demonstrate robust GRE signal at high field even with low flip angle (4–7°) and short T_R (12–36 ms).

The noise properties in tbSSFP also differ from conventional GRE imaging. The fit of the Krüger noise model to the SSFP data was relatively poor and may reflect the presence of different noise processes than are found in conventional GRE imaging. Respira-

tion-induced frequency shifts are known to be manifested differently in tbSSFP, as they can cause the underlying tissue frequency to shift relative to the reference frequency, causing the banding patterns to shift across the brain (Lee et al., 2006). Prospective noise reduction methods for SSFP have been developed which track and compensate for temporal drift in resonance frequency (Lee et al., 2006; Wu et al., 2007). These methods acquire real-time measurements of the frequency shift and feed this into the RF phase increment scheme so that, although the absolute frequency may drift, the SSFP banding patterns remain stationary. These methods reduce time series noise without affecting functional contrast, increasing the statistical significance of transition band SSFP FMRI. A similar study of the temporal SNR during real-time frequency tracking would be useful for studying the utility of these methods.
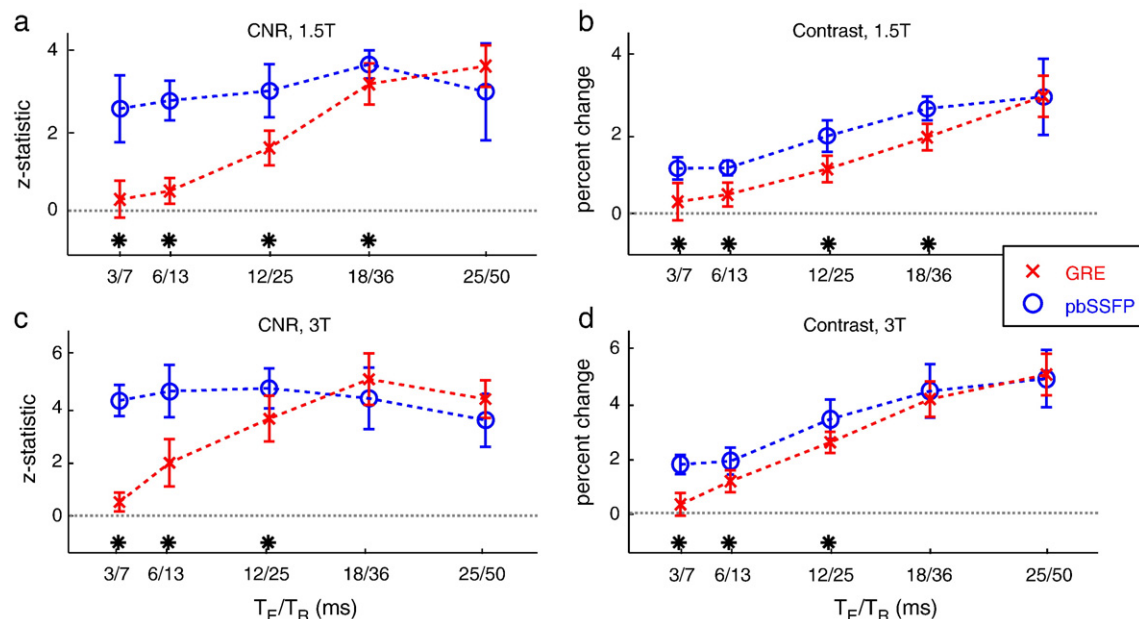
Fig. 7. Group results of functional contrast (b, d) and contrast-to-noise ratio (a, c) in the matched passband SSFP vs. GRE study over the range of T_E/T_R studied. The top row are data at 1.5 T and the bottom row are data at 3 T. The left column plots CNR and the right plots ΔS (contrast). SSFP data are plotted in blue and GRE data in red. For each T_E/T_R condition, the inter-subject mean±SD is plotted. The plotted lines are the group means (mean of subject means) for each condition. Black asterisks indicate a significant difference between GRE and SSFP in each condition (determined using a 2-sample, unpaired t-test).
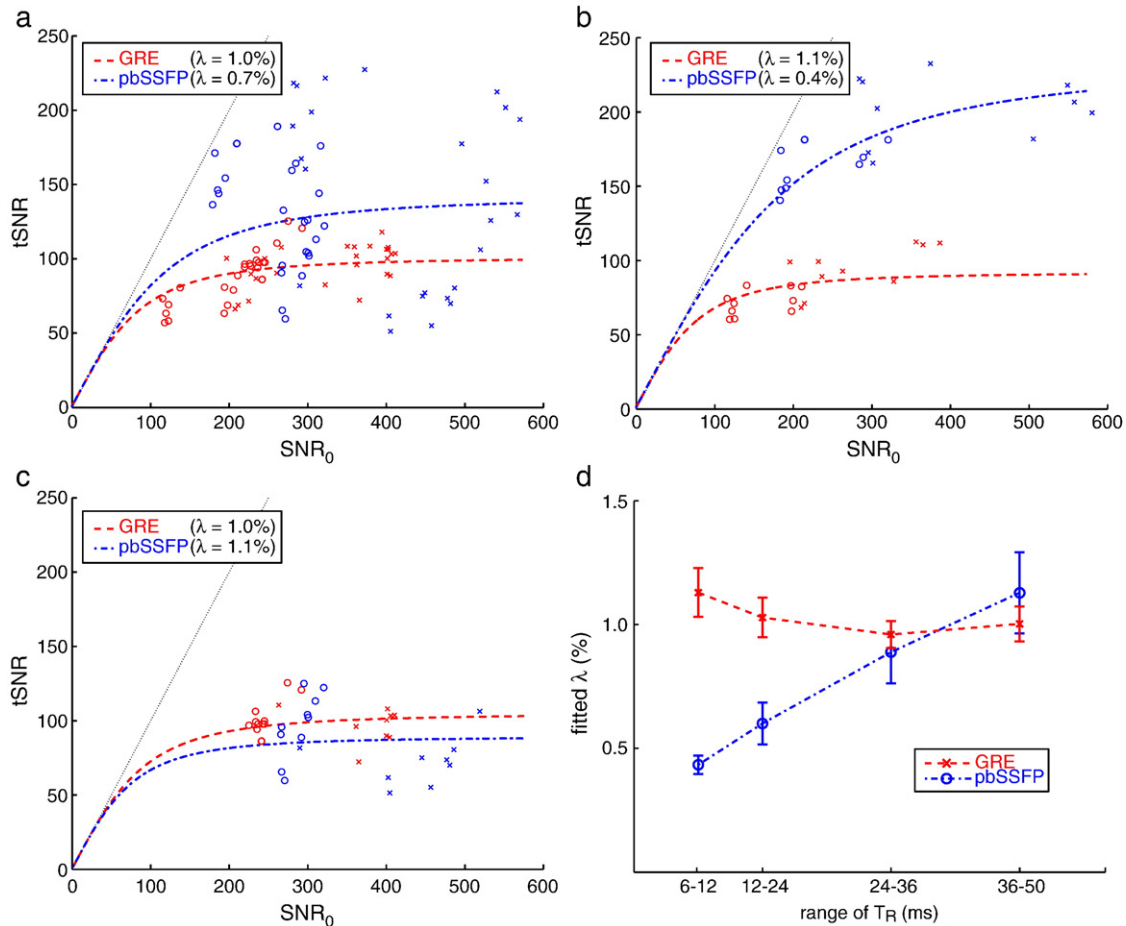
Fig. 8. Results of Krüger SNR model fitted to passband SSFP and GRE data. Individual points represent the mean for a single subject and single T_R over the functional ROI, with 1.5 T indicated by circles and 3 T indicated by crosses. The plots (a–c) differ in the range of T_R included in the data used in the fit. (a) When all data are included ($T_R = 6$–50 ms), the model provides a good fit to the GRE data, but a poor fit to the SSFP data. (b) When only the short T_R data are used ($T_R = 6$–12 ms), the model provides a good fit to the SSFP data with a small λ. (c) When only the long T_R data are used ($T_R = 36$–50 ms), the fitted λ for SSFP is similar to GRE, although the fit is noticeably poorer. (d) The value of λ fitted has a strong dependence on T_R for SSFP but not GRE.

Passband SSFP

Functional contrast in passband SSFP has only recently been reported (Bowen et al., 2005) and the mechanism of contrast has not yet been described. In our data, the GRE signal conforms to the familiar behavior of T_2^*-weighted functional signal, increasing linearly from zero contrast at $T_E = 0$. At long echo time, pbSSFP functional contrast converges with GRE functional signal, which likely indicates that the functional contrast arises due to T_2^* effects in the FID component of the SSFP signal. However, at short T_E/T_R, the SSFP signal diverges from GRE with functional contrast persisting even at very short T_E. Because our experimental protocol was designed to maximise the flatness of the SSFP passband, it is unlikely that much contrast will arise due to fluctuations in the SSFP signal profile (i.e., the kind of effects that are likely to dominate in transition band SSFP). One likely source of this contrast is from T_2 BOLD in stimulated echoes, which have a longer effective T_E than T_R. These signal changes would arise from diffusion of spins in the field disturbances surrounding deoxygenated blood vessels (Bowen et al., 2006), as occurs in more conventional spin-echo BOLD. There may also be a component of functional contrast that arises from water exchange

dynamics, as has previously been reported for whole blood (Dharmakumar et al., 2005).

The noise properties of passband SSFP have not previously been described, and the fits to the Krüger noise model have some important implications. First, the asymptotic limit for temporal SNR is considerably higher in pbSSFP at short T_R (i.e., λ is smaller), indicating less sensitivity to physiological noise than GRE. This is important to consider given the demonstrated reduction in contrast at short T_R (in the regime where T_2 effects are assumed to dominate). Second, reduced physiological sensitivity is not a general property of pbSSFP, as the physiological noise increases with T_R to eventually match, or potentially even exceed, that of GRE. The dependence of noise sensitivity on T_R cannot be simply explained due to the changing T_E in our experiment, since the GRE data with matched T_E and T_R has only minor dependence on T_R. The fits shown in Fig. 8d suggest that pbSSFP may tend to higher physiological noise sensitivity at long T_R, which may indicate similar noise amplification to that found in tbSSFP (due to an increase in banding). In this case, it may be beneficial to apply frequency tracking methods (Lee et al., 2006) to pbSSFP. The relatively flat CNR curves for pbSSFP shown in Figs. 7a and c reflect the fact that both physiological noise and functional contrast

increase with T_R. This property may be useful for optimising pbSSFP since short T_R acquisitions will both reduce banding artifacts and image distortion.

Conclusions

The passband SSFP technique has been shown to be consistent with contrast that changes from T_2 BOLD at short T_E/T_R to T_2^* BOLD at long T_E/T_R. The transition band SSFP technique also appears to exhibit significant T_2^* BOLD contrast at long T_E/T_R, but at short times exhibits high contrast that is more consistent with sensitivity of transition band SSFP to the deoxyhemoglobin frequency shift. SSFP has also been shown to exhibit different sensitivity to physiological noise. The physiological noise in passband SSFP is lower than GRE at low T_R and comparable to GRE at long T_R, which is likely related to the passband contrast mechanism. The physiological noise in transition band SSFP is considerably higher than GRE, presumably due to the known sensitivity of the transition band signal to respiratory-induced frequency drift.

Acknowledgments

Appendix A. Supplementary data

Supplementary data associated with this article can be found, in the online version, at doi:10.1016/j.neuroimage.2007.06.024.

References

Bowen, C., Menon, R., and Gati, J. (2005). High field balanced-SSFP FMRI: A BOLD technique with excellent tissue sensitivity and superior large vessel suppression. In Proc 13th ISMRM, page 119, Miami.

Bowen, C., Mason, J., Menon, R., and Gati, J. (2006). High field balanced-SSFP FMRI: Examining a diffusion contrast mechanism using varied flip angles. In Proc 14th ISMRM, page 665, Seattle.

Dharmakumar, R., Hong, J., Brittain, J.H., Plewes, D.B., Wright, G.A., 2005. Oxygen-sensitive contrast in blood for steady-state free precession imaging. Magn. Reson. Med. 53 (3), 574–583.

Dharmakumar, R., Hong, J., Wright, G.A., 2006. Detecting microcirculatory changes in blood oxygen state with steady-state precession imaging. Magn. Reson. Med. 55 (6), 1372–1380.

Gudbjartsson, H., Patz, S., 1995. The Rician distribution of noisy MRI data. Magn. Reson. Med. 34, 910–914.

Hennig, J., 1991. Echoes: How to generate, recognize, use or avoid them in MR-imaging sequences. Concepts Magn. Reson. 3, 125–143.

Krüger, G., Glover, G.H., 2001. Physiological noise in oxygenation-sensitive magnetic resonance imaging. Magn. Reson. Med. 46 (4), 631–637.

Lee, J., Santos, J.M., Conolly, S.M., Miller, K.L., Hargreaves, B.A., Pauly, J.M., 2006. Respiratory-induced B_0 field fluctuation compensation in balanced SSFP: Real-time approach for transition-band SSFP FMRI. Magn. Reson. Med. 55, 1197–1201.

Miller, K.L., Hargreaves, B.A., Lee, J., Ress, D., deCharms, R.C., Pauly, J.M., 2003. Functional MRI using a blood oxygenation sensitive steady state. Magn. Reson. Med. 50, 675–683.

Miller, K.L., Smith, S.M., Jezzard, P., Pauly, J.M., 2006. High-resolution FMRI at 1.5 T using balanced SSFP. Magn. Reson. Med. 55, 161–170.

Reeder, S.B., Herzka, D.A., McVeigh, E.R., 2004. Signal-to-noise ratio behavior of steady-state free precession. Magn. Reson. Med. 42, 123–130.

Scheffler, K., Hennig, J., 2003. Is trueFISP a gradient-echo or spin-echo sequence? Magn. Reson. Med. 49, 395–397.

Scheffler, K., Seifritz, E., Bilecen, D., Venkatesan, R., Hennig, J., Deimling, M., Haacke, E.M., 2001. Detection of BOLD changes by means of a frequency-sensitive TrueFISP technique: Preliminary results. NMR Biomed. 14, 490–496.

Smith, S.M., Jenkinson, M., Woolrich, M.W., Beckmann, C.F., Behrens, T.E.J., Johansen-Berg, H., Bannister, P.R., Luca, M.D., Drobnjak, I., Flitney, D.E., Niazy, R.K., Saunders, J., Vickers, J., Zhang, Y., Stefano, N.D., Brady, J.M., Matthews, P.M., 2004. Advances in functional and structural MR image analysis and implementation as FSL. NeuroImage 23, S208–S219.

Triantafyllou, C., Hoge, R.D., Krueger, G., Wiggins, C.J., Potthast, A., Wiggins, G.C., Wald, L.L., 2005. Comparison of physiological noise at 1.5 T, 3 T and 7 T and optimization of fMRI acquisition parameters. NeuroImage 26, 243–250.

Wu, M.L., Wu, P.H., Huang, T.Y., Shih, Y.Y., Chou, M.C., Liu, H.S., Chung, H.W., Chen, C.Y., 2007. Frequency stabilization using infinite impulse response filtering for SSFP FMRI at 3 T. Magn. Reson. Med. 57, 369–379.

Zhong, K., Leupold, J., Hennig, J., Speck, O., 2007. Systematic investigation of balanced steady-state free precession for functional MRI in the human visual cortex at 3 Tesla. Magn. Reson. Med. 57 (1), 67–73.